Medical Oncology (2025) 42:270
https://doi.org/10.1007/s12032-025-02793-3

ORIGINAL PAPER

Entinostat and novel analogs: preclinical evidence for anti-proliferative activity in adult T-cell leukemia/lymphoma

Sajad Goudarzi[1,2] · Zahra Nasiri Sarvi[1,3] · Hossein Ayatollahi[2] · Razieh Ghodsi[4,5] · Zeinab Noroozi[3] · Mohammad Reza Keramati[2] · Fatemeh B. Rassouli[1,3]

Received: 12 February 2025 / Accepted: 15 May 2025

Abstract

Adult T-cell leukemia/lymphoma (ATLL) has low overall survival, underscoring the need for the development of novel approaches. Present study aimed to investigate anti-proliferative effects of entinostat and its newly synthesized analogs on ATLL cells. Computational analyses were conducted to identify the potential molecular targets of entinostat, and construct a protein–protein interaction network. Then, enrichment analyses were performed, and the expression of CDK4 was assessed in MT-2 cells. Molecular docking and dynamics simulations were carried out to predict the interactions of entinostat and its novel analogs with target proteins. For *in vitro* studies, at first quinoline-based benzamide derivatives were synthesized. Then, MT-2 and normal cells were treated and their proliferation was evaluated by alamarBlue assay. Finally, flow cytometry was performed, and the expression of candidate genes was assessed by real-time PCR. Exploring potential targets of entinostat and pathogenic targets of ATLL revealed 51 overlapping molecules including CDK4. Volcano plot revealed over expression of CDK4 in MT-2 cells. Favorable and stable binding of entinostat and its analogs with the activation loop of CDK4 and the CDK-binding site of cyclin D1 was confirmed. Experimental studies revealed anti-proliferative effects of entinostat and analogs on MT-2 cells, confirmed by flow cytometry analysis and alterations in the expression of *BAX*, *CCND1*, and *BCL-2*. Present findings pave the way for the development of new drugs against ATLL, and provide evidence that justifies further preclinical evaluations of entinostat and its novel analogs.

Keywords Adult T-cell leukemia/lymphoma · Entinostat · Novel analogs · Anti-proliferative effect · CDK4

Introduction

Adult T-cell leukemia/lymphoma (ATLL) is a highly aggressive peripheral T-cell malignancy that occurs in individuals infected with human T-cell lymphotropic virus type 1 (HTLV-1), an oncogenic retrovirus [1]. HTLV-1 is prevalent in specific regions worldwide, including Taiwan, Japan, the Caribbean, Central and South Africa, and some areas of the Middle East, such as Northeast Iran [2–4]. HTLV-1 transmission primarily occurs through breastfeeding, sexual contact, blood products, and organ transplants. Most HTLV-1 carriers remain asymptomatic, and a minority of infected individuals develop symptomatic conditions such as ATLL and autoimmune disorders. HTLV-1 can also contribute to co-infections with HIV, tuberculosis and chronic infective dermatitis [5]. ATLL is classified into four subtypes including acute, chronic, smoldering and lymphomatous. The median survival for chronic and smoldering ATLL is approximately 2–5 years, while for acute and lymphomatous

Sajad Goudarzi and Zahra Nasiri Sarvi have contributed equally to this work.

✉ Fatemeh B. Rassouli
behnam3260@um.ac.ir

1 Novel Diagnostics and Therapeutics Research Group, Institute of Biotechnology, Ferdowsi University of Mashhad, Mashhad, Iran

2 Cancer Molecular Pathology Research Center, Department of Hematology and Blood Bank, Faculty of Medicine, Mashhad University of Medical Sciences, Mashhad, Iran

3 Department of Biology, Faculty of Science, Ferdowsi University of Mashhad, Mashhad, Iran

4 Biotechnology Research Center, Pharmaceutical Technology Institute, Mashhad University of Medical Sciences, Mashhad, Iran

5 Department of Medicinal Chemistry, School of Pharmacy, Mashhad University of Medical Sciences, Mashhad, Iran

Published online: 17 June 2025

forms it is less than a year. Acute ATLL accounts for less than 50% of cases, and the overall survival rates for acute, chronic, lymphomatous and smoldering ATLL are 11%, 36%, 14% and 52%, respectively [6]. Currently, there are several chemotherapeutic approaches for treating ATLL, such as zidovudine and interferon-alpha (AZT/IFN) antiviral therapy for chronic and smoldering ATLL with overall response rate of 58% that extends overall survival by 6–18 months [7, 8]. The poor prognosis of ATLL is largely attributed to the emergence of drug resistance and severe immunosuppression, underscoring the need for the development of innovative therapeutic approaches.

As the main oncoprotein of HTLV-1, Tax plays a critical role in leukemogenesis by activating multiple cellular pathways and increased expression of viral genes [9, 10]. Tax promotes T-cell immortalization by disrupting cell cycle regulation and enhancing clonal proliferation. It upregulates cyclin-dependent kinase 4 (CDK4) and its regulatory partner cyclin D1 (CCND1), accelerating the G_1/S-phase transition and cell cycle progression [11, 12]. A clinical study reported that CDK4 is significantly overexpressed in ATLL patients, with this increase closely associated with disease progression [13]. Mechanistically, Tax impairs cyclin-dependent kinase inhibitors like p16INK4A and directly interacts with CDK4 and cyclin D1, boosting CDK4 kinase activity and making the CDK4/cyclin D complex resistant to p21CIP inhibition [14, 15]. Furthermore, Tax activates transcription factors such as nuclear factor kappa-light-chain-enhancer of activated B cells (NF-κB) and cAMP response element-binding protein (CREB), which upregulate CCND1 expression, driving abnormal T-cell proliferation and ATLL development [16]. Tax-mediated constitutive activation of NF-κB also induces multiple antiapoptotic genes such as BCL-2 family members that promote cell survival [17], and inhibition of BCL-2 has been shown to induce apoptosis in ATLL cells [18]. ATLL cells also exhibit elevated levels of the pro-apoptotic protein BAX, increasing their sensitivity to apoptosis-inducing agents like Navitoclax [19]. Paradoxically, while high BAX expression may facilitate apoptosis, it is also linked to genomic instability and lymphoma progression, as observed in T-cell malignancies [20].

Histone deacetylases (HDACs) play significant roles in the epigenetic regulation by removing acetyl groups from lysine residues on histone proteins, leading to gene expression. There are four classes of human HDACs, with most being zinc- or NAD^+-dependent. Overexpression of HDACs can contribute to the development of malignant features such as angiogenesis, migration and invasion in neuroblastoma, pancreatic, colorectal and lung carcinomas [21, 22]. Due to the impact of HDACs on cancer progression, various HDAC inhibitors (HDACis) are being explored as potential therapeutic molecules. These inhibitors have shown the ability to induce apoptosis, autophagy, cellular senescence, oxidative stress, DNA damage, and enhance the immune system [23]. To note, a number of HDACis have received FDA approval for different hematological malignancies except ATLL [24–27].

Entinostat ($C_{21}H_{20}N_4O_3$), also known as SNDX-275, selectively targets class I and IV HDACs, promoting histone hyperacetylation and activation of genes associated with terminal differentiation and apoptosis. Entinostat has been extensively studied in clinical trials for the treatment of breast carcinoma, and has shown potential anticancer effects in multiple myeloma, leukemia, colon and esophageal carcinomas [28–32]. As a hydroxamate HDACi, the structure of entinostat consists of a benzamide moiety that acts as the zinc-binding domain (ZBD), a pyridine ring that functions as the surface recognition domain, and a phenyl ring that acts as the hydrophobic linker. In this study, we introduced a quinoline scaffold as the cap group, given its well-established role in anticancer drug development and its potential to enhance anti-proliferative activity. Based on this, we designed two novel analogs, further modified by incorporating a 4-(aminomethyl) benzamide linker at the 4-position of the quinoline ring and using o-phenylenediamine as ZBD. These structural modifications were intended to explore whether such changes could improve the biological efficacy and selectivity of the parent compound, entinostat.

Due to the dismal outcomes of available therapeutic approaches, there is an urgent need to develop novel and more efficacious strategies to improve long-term survival in ATLL patients. Therefore, this study aimed to investigate for the first time anti-proliferative effects of entinostat and newly synthesized analogs on ATLL cells. Initially, computational analyses were performed to identify the potential molecular targets of entinostat as well as pathogenic targets of ATLL, and protein–protein interaction (PPI) network was constructed for overlapping targets. Then, pathway enrichment analyses were performed and the expression of CDK4 was assessed in MT-2 cells using Gene Expression Omnibus (GEO) database. Molecular docking and dynamics simulations were also carried out to predict the interaction of entinostat and novel analogs with CDK4 and cyclin D1. For in vitro studies, proliferation of ATLL and normal cells was evaluated by alamarBlue assay upon treatment with entinostat and analogs, and flow cytometry was carried out to detect apoptosis. To gain insights into the molecular mechanism of observed effects, real-time PCR was performed to assess the expression of candidate genes.

Materials and methods

In situ studies

Target prediction of entinostat and ATLL

SwissTargetPrediction database (https://www.swisstargetprediction.ch) was used to provide a library of entinostat protein targets using the SMILE code obtained from PubChem (https://pubchem.ncbi.nlm.nih.gov/). In addition, ATLL-associated genes were obtained from GeneCards database (https://www.genecards.org/). Then, overlapping targets related to entinostat and ATLL were defined by Venn diagram (https://jvenn.toulouseinra.fr/app/example.html).

Protein–protein interaction and gene set enrichment analyses

PPI network of overlapping targets was acquired from STRING database (https://string-db.org/), and visualized by Cytoscape software (version 3.10.1) using CytoHubba 0.1 plugin. To assess the biological significance of overlapping targets, enrichment analyses was conducted by STRING and results yielded false discovery rate (FDR) in terms of Kyoto Encyclopedia of Genes and Genomes (KEGG) pathways and WikiPathways.

Data collection from GEO

To find gene expression datasets for ATLL cells, GEO (http://www.ncbi.nlm.nih.gov/geo) was used as a public repository containing high-throughput functional genomic data. Key words were 'MT-2' and 'normal lymphocyte' and the study type was 'Expression profiling by array'. GSE6034 dataset was selected for further examination, and microarray data were obtained from GPL570 platform. Data were analyzed in R (version 4.4.0) using "GEOquery" and "limma" packages, with p-values adjusted using the Benjamini & Hochberg method for controlling the FDR (cut-off level $=0.05$). The volcano plot was drawn using the "ggplot2" package in R with p-value <0.05 and $\log_2$ fold-change ($\log_2$FC) >1).

Molecular docking

To assess the potential binding between entinostat and analogs with CDK4 and cyclin D1, molecular docking was performed. The three-dimensional structure of entinostat (ID: 4261) was obtained from PubChem (https://pubchem.ncbi.nlm.nih.gov/), while the structures of novel analogs were created by ChemInfo (https://www.cheminfo.org/) and NovoPro Bioscience (https://www.novoprolabs.com/) online tools, and ligand preparation was performed by energy minimization in Avogadro 2. The crystal structures of CDK4 (ID: 3g33) and cyclin D1 (ID: 2w96) were obtained from Protein Data Bank (https://www.rcsb.org/). Proteins Plus (https://proteins.plus/) was employed for molecular structure optimization and docking studies [33]. Molecular docking was performed using the JAMDA tool, which estimates the stability and specificity of protein–ligand complexes by calculating binding free energies [34]. The resulting docking poses and interactions were analyzed and visualized in both two- and three-dimensional formats using PoseEdit and PoseView, facilitating comprehensive interpretation of molecular interactions [35, 36].

Molecular dynamics simulations

To assess the conformational flexibility and binding stability of the entinostat–CDK4 complex, molecular dynamics simulations were performed. The simulations were performed using GROMACS (version 2023) with the CHARMM36 all-atom force field. A Bash script was created to streamline the preparation steps, including merging, solvation, energy minimization, and equilibration of protein–ligand topologies. The complex was solvated with TIP3P water molecules under CHARMM parameters, and counterions (Cl^-/Na^+) were added to neutralize the system, followed by energy minimization until atomic forces reached <10 kJ/mol. Sequential equilibration involved NVT (constant particles, volume, temperature) and NPT (constant particles, pressure, temperature) phases, maintaining 310 K and 1 bar with Parrinello-Rahman coupling. Subsequent production simulations extended to 100 ns using the leapfrog integrator (2 fs timestep). Trajectory analysis included evaluating structural stability via root mean square deviation (RMSD), residue flexibility via root mean square fluctuation (RMSF), compactness via radius of gyration (Rg), surface solvent interactions via solvent accessible surface area (SASA), and intermolecular forces via Coulombic and Lennard–Jones potentials. Results were plotted using the ggplot2 package in R.

In vitro studies

Synthesis of analogs

Entinostat was purchased from Sigma-Aldrich. Two quinoline-based benzamide derivatives (Fig. 1), N-(4-((2-aminophenyl)carbamoyl)benzyl)−6,7-dimethoxy-2-methylquinoline-4-carboxamide (analog 1) and N-(2-aminophenyl)−2-(4-fluorophenyl)quinoline-4-carboxamide (analog 2), were synthesized as recently described [37, 38]. Briefly, the synthesis of analog 1 was started by the

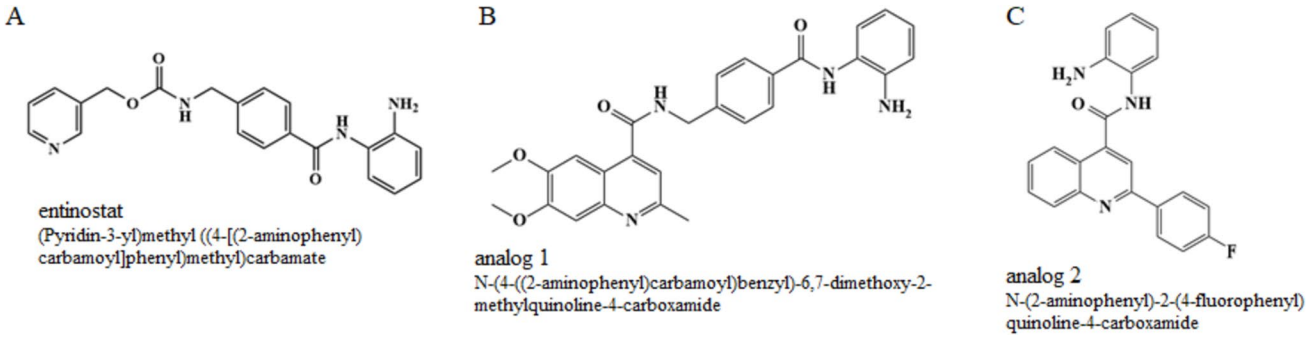

Fig. 1 Chemical structure of entinostat (**A**), analog 1 (**B**) and analog 2 (**C**)

production of a 2-methylquinoline-4-carboxylic acid derivative coupled with 4-(aminomethyl) benzoic acid. Then, an imidazole intermediate was formed and the reaction was continued with adding o-phenylenediamine to obtain analog 1. Similarly, the reaction between a quinoline-4-carboxylic acid derivative with o-phenylenediamine led to the synthesis of analog 2.

Characterization of analogs

The chemical structures of both analogs were characterized by ^{1}H NMR and ^{13}C NMR spectra (Bruker FT-300 MHz instrument), infrared (IR) spectra (Perkin Elmer Model 1420 spectrometer) and mass spectra (A 3200 QTRAP LC/MS triple quadrupole mass spectrometer).

Characterization of analog 1 was as follow: white solid; yield: 88%; melting point: 242 °C; IR (KBr): νmax 3386 and 3303 (NH and NH_2), 1643 and 1506 (CO); ^{1}H NMR (300 MHz, DMSO-d_6) δ 9.69 (s, 1H, NH), 9.35 (t, J = 6.0 Hz, 1H, NH), 8.04 (d, J = 8 Hz, 2H, Ar–H), 7.58 (d, J = 8 Hz, 2H, Ar–H), 7.45 (s, 1H, Ar–H), 7.40 (m, 2H, Ar–H), 7.27–7.18 (m, 1H, Ar–H), 7.02 (td, J = 7.5, 1.5 Hz, 1H, Ar–H), 6.83 (dd, J = 8, 1.5 Hz, 1H, Ar–H), 6.65 (td, J = 7.5, 1.5 Hz, 1H, Ar–H), 4.94 (s, 2H, NH_2), 4.65 (d, J = 6.0 Hz, 2H, CH_2), 3.96 (s, 3H, OCH_3), 3.82 (s, 3H, OCH_3), 2.66 (s, 3H, CH_3). ^{13}C NMR (75 MHz, DMSO-d_6) δ 167.76, 165.60, 156.09, 152.60, 149.67, 145.54, 143.63, 143.28, 140.52, 133.83, 128.46, 127.68, 127.20, 127.00, 123.85, 118.22, 116.81, 116.66, 108.17, 103.35, 56.15, 55.88, 42.87, 24.89. LCMS (ESI, m/z): 471 $[M+1]^{+}$, 493 $[M+23]^{+}$. ^{1}H NMR, ^{13}C NMR, IR, and mass spectra for analog 1 are provided in Supplementary Information (S1).

Characterization of analog 2 was as follow: cream solid; yield: 59%; melting point: 199–204 °C; IR (KBr): νmax (cm-1) 3401, 3332 and (NH and.

NH2) and 1672 (CO); ^{1}H NMR (300 MHz, DMSO-*d*6) δ 10.09 (s, 1H, NH), 8.56–8.37 (m,

3H, Ar–H), 8.30 (dd, J = 8.5, 1.4 Hz, 1H, Ar–H,), 8.23–8.16 (m, 1H, Ar–H), 7.88 (ddd, J =

8.5, 6.8, 1.5 Hz, 1H, Ar–H), 7.71 (ddd, J = 8.3, 6.8, 1.3 Hz, 1H, Ar–H), 7.46 (t, J = 8.8 Hz,

3H, Ar–H), 7.06 (td, J = 7.6, 1.6 Hz, 1H, Ar–H), 6.87 (dd, J = 8.1, 1.5 Hz, 1H, Ar–H), 6.69.

(td, J = 7.5, 1.5 Hz, 1H, Ar–H), 5.14 (s, 2H, NH2). ^{13}C NMR (75 MHz, DMSO-*d*6) δ 163.92.

(1JCF = 245.25 Hz), 162.29, 155.27, 148.37, 143.66, 143.41, 135.27 (4JCF = 3 Hz), 130.74,

130.16 (3JCF = 8.25 Hz), 130.02, 127.55 (2JCF = 30 Hz), 127.01, 125.85, 123.90, 122.92,

117.44, 116.63, 116.50, 116.45, 116.16. LCMS (ESI, m/z): 358 [M + 1] +. ^{1}H NMR, ^{13}C NMR, IR, and mass spectra for analog 2 are provided in Supplementary Information (S2).

Cell culture, treatment and proliferation assay

The present study utilized HTLV-1-transformed human T cells (MT-2 cell line) and normal human cells (HFF-3 cell line), both obtained from the Pasteur Institute (Tehran, Iran). MT-2 cells were cultured in Roswell Park Memorial Institute-1640 medium (Capricorn), while HFF-3 cells were maintained in high-glucose Dulbecco's modified Eagle's medium (Capricorn); both media were supplemented with 10% fetal bovine serum (Gibco), 0.1% L-glutamine (Gibco), and 1% penicillin/streptomycin (Sigma). All cells were incubated at 37 °C in a humidified atmosphere with 5% CO_2.

To assess the effects of agents, at first stock solutions of entinostat (MW: 376.4 g/mol), analog 1 (MW: 468 g/mol) and analog 2 (MW: 357 g/mol) were prepared using dimethyl sulfoxide (DMSO) as solvent, and final concentrations (12.5, 25 and 50 µM) were prepared using complete medium. Then, cells were seeded into 96-well plates (SPL) at a density of 50,000 cells/well and treated with increasing concentrations of entinostat and novel analogs for 24 and 48 h. At the end of each time point, proliferation of cells was evaluated by alamarBlue assay as a colorimetric test. To do so, alamarBlue reagent (0.1 mg/ml, Sigma) was added to each well (10% v/v) and cells were incubated at

37℃ for 3 h. Then, absorbance (A) was measured at 600 nm (Epoch Biotek) and proliferation (%) was calculated using the following equation: 100-(AT-AU/AB-AU)*100, where T, U and B represent treated cells, untreated cells and blank control, respectively.

Detection of apoptosis

To detect cell apoptosis, annexin V-fluorescein isothiocyanate (FITC) and propidium iodide (PI) staining was performed. Briefly, upon 24 h treatment with 50 µM entinostat and analogs, cells were collected and washed twice with PBS. Subsequently, the cell pellet was resuspended in binding buffer containing annexin V-FITC and PI (MabTag) and incubated at room temperature for 15 min. Finally, flow cytometry was performed using FL1-H and FL2-H filters (BD FACSCaliber) and results were analyzed by Flow Jo software.

Real-time PCR

The expression of *CD44*, *CCND1*, *BAX*, and *BCL-2* was assessed by real-time PCR. Briefly, cells were treated with 50 µM entinostat and analogs for 24 h and RNA was extracted following the manufacture's instruction (DENA Zist). Upon confirming the purity of RNA spectrophotometrically (Thermofisher), cDNAs were synthesized by reverse transcription using oligo dT, random hexamer and M-MuLV reverse transcriptase according to the manufacturer's protocol (Thermo Scientific). Real-time PCR was performed in Rotor Gene 6000 cycler using SYBR green master mix (Biofact) and primers listed in Table 1. PCR conditions were defined as holding at 94 °C for 5 min, followed by 36 cycles of 95 °C for 20 s, 58 °C for 30 s and 72 °C for 30 s.

Statistical analysis

The data were analyzed statistically by one-way ANOVA in GraphPad Prism software. Results are presented as mean ± SD, and statistical significance was considered for $p < 0.05$, < 0.01, < 0.001, and < 0.0001.

Results

CDK4 was recognized as a therapeutic target with important interactions and functions

Through screening the targets from GeneCards database, a total of 3357 potential targets associated with ATLL were identified. These targets were then analyzed with targets of entinostat obtained from the SwissTargetPrediction database. Venn diagram was constructed (Fig. 2-A), and a total of 51 overlapping targets were emerged including CDK4, and the PPI network was constructed by STRING and Cytoscape. As shown in Fig. 2-B-C, 50 nodes in the network were interconnected by 230 edges. Then, CytoHubba identified the top ten hub genes by DMNC method, and CDK4 was ranked as the sixth. Pathway enrichment analyses were conducted for ten hub targets and results demonstrated significant terms in various categories (Fig. 2-D-E). *Viral carcinogenesis* (FDR: 2.73e-10) in KEGG pathways, and *Cell cycle* (FDR: 4.54e-07) in WikiPathways were identified among the most significant terms.

Gene expression analysis revealed upregulation of CDK4 in MT-2 cells

Since CDK4 was among the overlapped targets for ATLL and entinostat with significant interactions and functions, we then explored the expression of CDK4 in MT-2 cells using GSE6034 dataset. As presented in Fig. 3, the volcano plot generated for MT-2 cells demonstrated over expression of CDK4.

Entinostat and novel analogs exhibited favorable and stable interactions with CDK4 and cyclin D1

To define whether entinostat and novel analogs could interact with CDK4 and cyclin D1 and affect the proliferation of ATLL cells, molecular docking was performed. The optimal binding pocket for CDK4 was identified within its activation loop, whereas for cyclin D1, it was located at the CDK4 binding site. The cavities that exhibited the highest affinity score were subsequently chosen for the calculation of the minimum docking binding energy. As illustrated

Table 1 List of primers used for real-time PCR analysis in current study

Gene	Length (bp)	Forward (5′ → 3′)	Reverse (5′ → 3′)
TBP	120	ACAACAGCCTGCCACCTTA	GAATAGGCTGTGGGGTCAGT
BCL-2	124	GATGACTGAGTACCTGAACATGG	CAGAGACAGCCAGGAGAAATC
BAX	150	GGACGAACTGGACAGTAACATGG	GCAAAGTAGAAAAGGGCGACAAC
CCND1	151	TGAAGGAGACCATCCCCTG	TGTTCAATGAAATCGTGCGG
CD44	176	CGGACACCATGGACAAGTTT	GAAAGGCCTTGCAGAGGTCAG

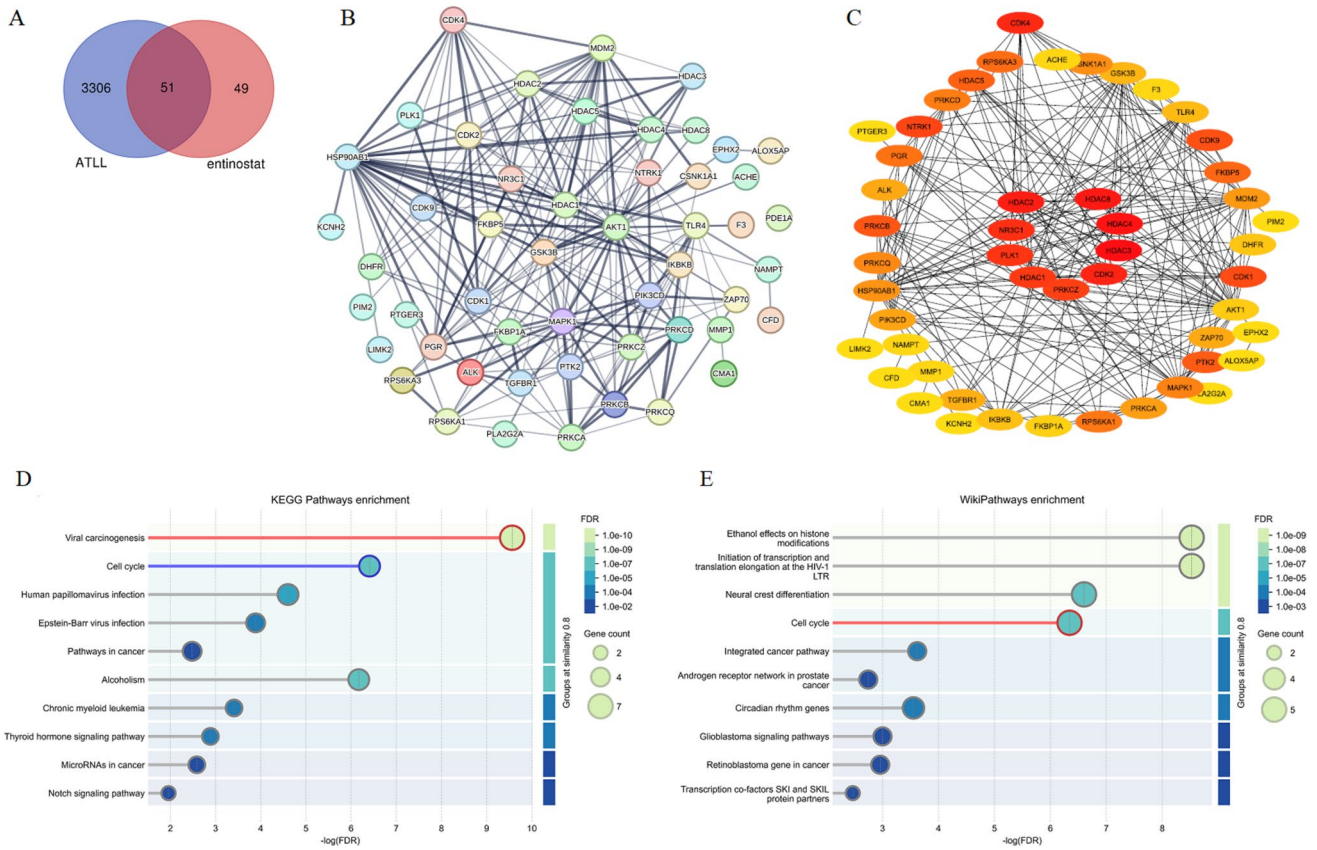

Fig. 2 Identification of CDK4 as a hub target with multiple interactions and functions. Venn diagram illustrates the overlap of 51 target genes between ATLL and entinostat (**A**). The PPI network, constructed using STRING, depicts functional associations among the overlapping targets (**B**). Cytoscape visualization of the PPI network highlights ten hub genes, with node colors reflecting expression levels from significantly high (red) to low (yellow) (**C**). Pathway enrichment analyses were performed on top 10 hub genes to determine the most significant terms in KEGG pathways (**D**) and WikiPathways (**E**)

in Fig. 4 and summarized in Table 2, entinostat interacted with the activation loop of CDK4 through hydrogen bonds with Tyr22, Gln173, Ala175, Leu176 and Thr177 and several hydrophobic contacts, exhibiting a binding affinity of −2.757 JAMDA score. In addition, entinostat interacted with cyclin D1 through hydrogen bonds with Arg87, Lys149 and Trp150, with a favorable binding affinity of −2.608 JAMDA score. The interaction between analog 1 and CDK4 was also stable and involved hydrogen bonds with Ala21, Ala175, Tht177 and Arg186 and multiple hydrophobic contacts with a binding affinity of − 2.986 JAMDA score. Likewise, binding position of analog 2 was predicted within the activation loop of CDK4 and the best pose show suitable binding affinity with a JAMDA score of −2.301. In addition, the interactions between analog 1 and analog 2 with cyclin D1 exhibited binding energies of − 2.57 and − 2.065 JAMDA score, respectively.

The dynamic behavior of the interaction between entinostat and CDK4 was examined, focusing on stability and structural integrity (Fig. 5). The RMSD of the entinostat-CDK4 complex ranged from 0.005 to 3.437 Å, indicating stable ligand binding with rotational flexibility within the CDK4 activation loop. The RMSF analysis revealed that CDK4 in complex with entinostat exhibited fluctuation predominantly below 3.928 Å, suggesting minimal structural disruption. The analysis of Rg confirmed consistent structural compactness, indicating maintained overall integrity of the complex. Assessment of changes in hydrophilic and hydrophobic residues by SASA yielded an average value of 152.13 nm^2 for the complex, highlighting significant solvent exposure of the protein surface, which may facilitate ligand binding. Additionally, Coulombic and Lennard–Jones potential analyses demonstrated sustained interaction between CDK4 and entinostat throughout the simulation, reinforcing the stability of their binding.

Entinostat and analogs induced anti-proliferative effects and apoptosis in MT-2 cells

As favorable interaction of entinostat and analogs with cell cycle regulators was determined by computational analyses, we then conducted in vitro studies to evaluate

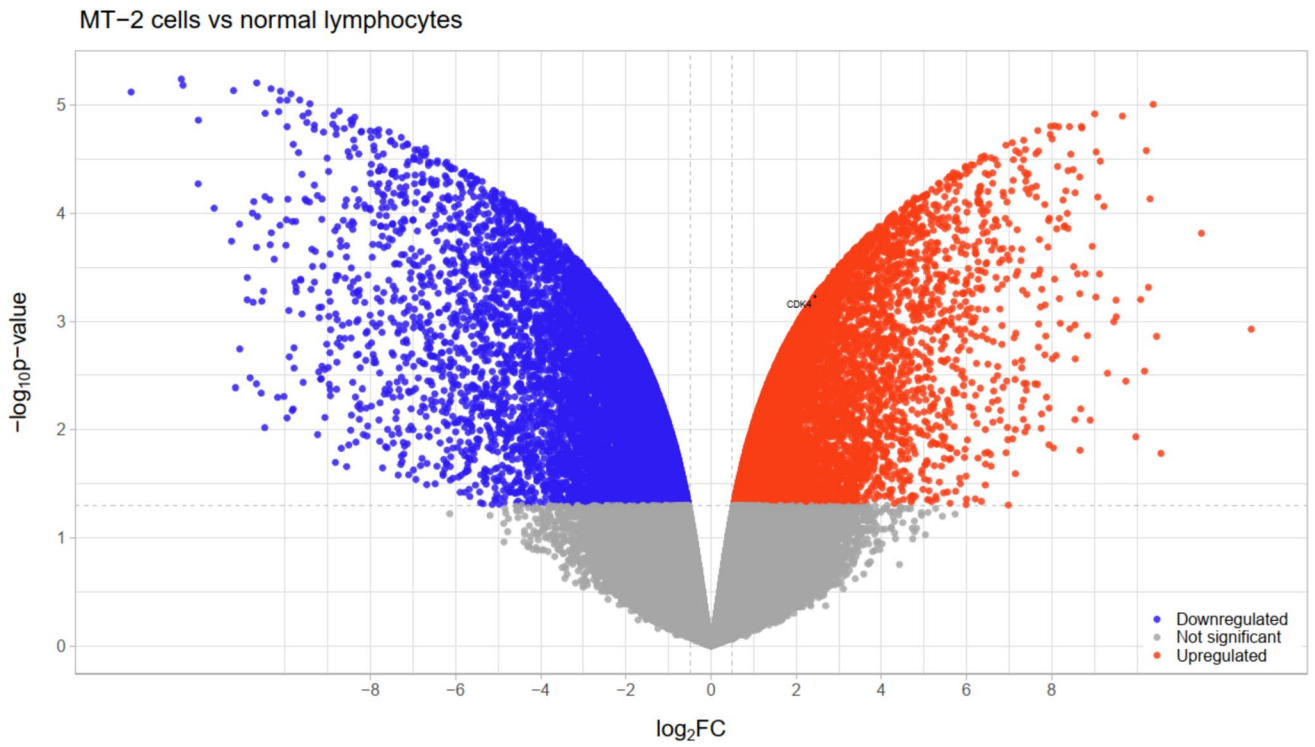

Fig. 3 Upregulation of CDK4 in MT-2 cells. Volcano plot visualize the expression of CDK4 in GSE6034 dataset (Platform GPL570). The plots utilize both *p*-values and log2 (fold-change) to identify differentially expressed genes in MT-2 cells. Colored dots showed genes with specific expression based on log2 FC (green dots), both adjusted *p*-value and log2 FC (red dots), and not significant in both terms (gray dots)

whether entinostat and novel analogs have the potential to affect the growth and survival of ATLL cells. As presented in Fig. 6-A-B, all three agents reduced the proliferation of MT-2 cells in a dose-dependent manner. The highest anti-proliferative effects were observed after 24 h, as treatment with 50 µM entinostat, analog 1 and analog 2 significantly ($p < 0.0001$) reduced proliferation down 54.3%, 65.5% and 60.8%, respectively. In addition, upon 48 h treatment with 50 µM entinostat, analog 1 and analog 2, cell proliferation was significantly ($p < 0.01$) decreased to 66.3%, 66.3% and 50.5%, respectively. Notably, entinostat and its analogs showed minimal effects on normal cells, with proliferation rates of 100%, 86.8%, and 84.6% following 48 h treatment with 50 µM entinostat, analog 1 and analog 2, respectively. Beside results of alamarBlue assay, flow cytometry analysis revealed induced apoptosis upon treatment with entinostat and analogs. Figure 6-C shows that, compared to the DMSO control group (10.4% apoptotic cells), 24 h treatment with 50 µM entinostat, analog 1, and analog 2 resulted in 26.2%, 11.7%, and 16.2% apoptotic cells, respectively. These results suggest that the effects observed in alamarBlue assay were mainly attributable to the anti-proliferative effects of entinostat and analogs rather than the induction of apoptosis.

Entinostat and analogs altered the expression of target genes

To unravel the molecular mechanism behind observed effects of entinostat and novel analogs, real-time PCR was carried out (Fig. 6D–G). Obtained results revealed significant ($p < 0.05$) down regulation of *BCL-2* upon treatment with analog 1 and analog 2. Additionally, up regulation of *BAX* and down regulation of *CCND1* by analog 1 and analog 2 were observed, although not significant. To note, the expression of *CD44* was not affected by the treatments.

Discussion

ATLL is a highly aggressive lymphocytic neoplasm with a prognosis that is typically poorer compared to other types of non-Hodgkin's lymphomas. Despite availability of multi-agent approaches, clinical outcomes are unsatisfactory due to intrinsic chemoresistance and severe immunosuppression. Therefore, the quest for novel and more efficacious regimes to ensure the long-term survival of ATLL patients remains a crucial focus of research.

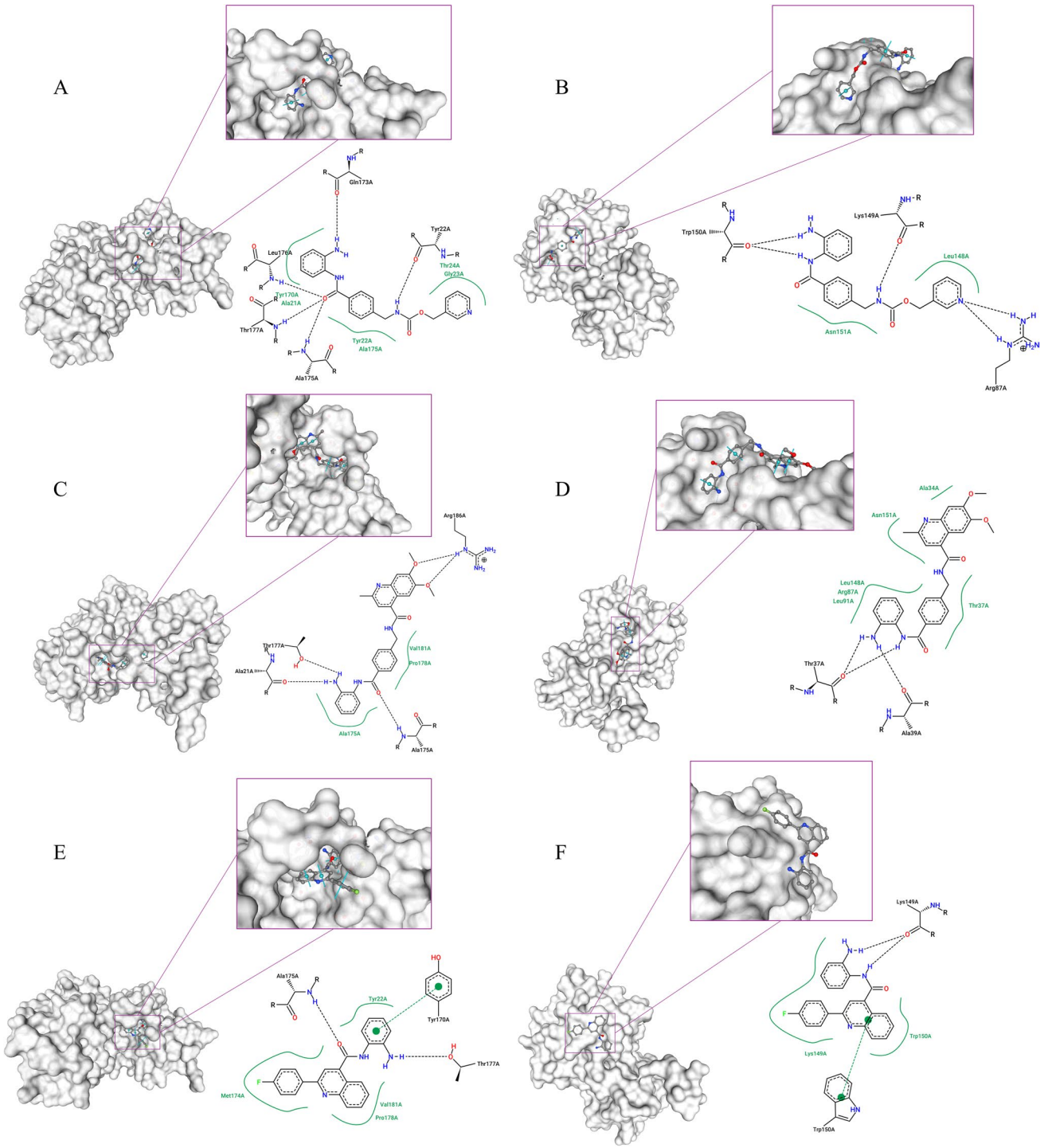

Fig. 4 Favorable interactions of entinostat and novel analogs with CDK4 and cyclin D1. Molecular docking diagrams of entinostat (**A** and **B**), analog 1 (**C** and **D**) and analog 2 (E and F) binding to the activation loop of CDK4 (**A**, **C** and **E**) and the CDK-binding site of cyclin D1 (**B**, **D** and **F**). 2D and 3D images were generated using PoseView

HDACs have elevated expression in various human neoplasms, and thus, the introduction of HDACis is of paramount importance in cancer treatment. HDACis regulate the intrinsic apoptosis pathway by increasing the expression of pro-apoptotic protein BAX and apoptosis-inducing ligand (TRAIL) receptors, while decreasing anti-apoptotic proteins BCL-2, BCL-XL, and Mcl-1, and pro-survival protein XIAP [39]. At the present time,

Table 2 Docking details of entinostat, analog 1 and analog 2 with CDK4 and cyclin D1

Protein	Ligand	Affinity (JAMDA score)	Hydrogen Bond & pi–pi interactions	Hydrophobic contacts
CDK4	entinostat	– 2.757	Tyr22—Gln173—Ala175—Leu176—Thr177	Ala21—Tyr22—Gly23—Thr24—Tyr170—Ala175
	analog 1	– 2.986	Ala21—Ala175—Thr177—Arg186	Ala175—Pro178—Val181
	analog 2	– 2.301	Tyr170—Ala175—Thr177	Tyr22—Met174—Pro178—Val181
cyclin D1	entinostat	– 2.608	Arg87—Lys149—Trp150	Leu148—Asn151
	analog 1	– 2.570	Thr37—Ala39	Ala34—Thr37—Arg87—Leu91—Leu148—Asn151
	analog 2	– 2.065	Lys149—Trp150	Lys149—Trp150

four HDACis have received FDA approval, including vorinostat (SAHA) for cutaneous T-cell lymphoma, belinostat (PXD101) for peripheral T-cell lymphoma, panobinostat (LBH589) for multiple myeloma and romidepsin (FK-228) for peripheral T-cell lymphoma [24–27]. Regarding entinostat, it has shown promising anti-tumor activity in Hodgkin lymphoma, acute myeloid leukemia (AML), chronic myelomonocytic leukemia and multiple myeloma [31, 32, 40, 41]. Since no study has yet determined the effects of entinostat on ATLL cells, the present research investigated anti-proliferative effects of entinostat on MT-2 cells for the first time. Additionally, based on the pivotal role of the quinoline scaffold in anticancer drug development, we synthesized two novel benzamide analogs incorporating this moiety as the cap group. These analogs were further structurally optimized by introducing a 4-(aminomethyl) benzamide linker, combined with o-phenylenediamine as the ZBD. This strategic modification aimed to refine the pharmacophore of entinostat, potentially improving its anti-proliferative efficacy against ATLL cells.

Exploring potential molecular targets of entinostat and pathogenic targets of ATLL revealed several overlapping targets including CDK4, which had high interactions in the PPI network. Enrichment analyses revealed various molecular functions for CDK4 and indicated its involvement in several biological pathways. Volcano plot generated from the expression profile of MT-2 cells revealed over expression of CDK4. Molecular docking provided insight into the action of entinostat and novel analogs, as binding of all three agents with the activation loop of CDK4 and the CDK-binding site of cyclin D1 were predicted with appropriate affinity. Additionally, molecular dynamics simulations confirmed the conformational flexibility and binding stability of the entinostat-CDK4 complex. To provide experimental evidence for the effects of entinostat and novel analogs on ATLL cells, the proliferation of MT-2 cells was assessed. The results indicated that all agents reduced proliferation of cells in a dose-dependent manner. Flow cytometry analysis revealed that observed effects of entinostat and analogs were, to some extent, due to the induction of apoptosis, as also indicated by alterations in the expression of *BAX*, *CCND1*, and *BCL-2*.

Our findings are in consistence with previous reports, which indicated anti-proliferative and apoptosis-inducing effects of entinostat on Hodgkin lymphoma cell lines were mediated via altering the expression of P21, BCL-2 and BCL-xL without affecting Mcl-1 or BAX levels. Additionally, entinostat modulated cytokine levels, including interleukin-12 p40-70, interleukin-13, interleukin-4 and CXCL10 [41]. It has also been reported that entinostat induced apoptosis in AML cells through induction of c-Jun, JunB, death receptor TRAIL and pro-apoptotic proteins BIM and Noxa [42]. Combinatorial effects of entinostat and fludarabine were also investigated on chronic lymphocytic leukemia (CLL) cells, and results revealed induction of apoptosis through upregulation of BAX and downregulation of HDAC1, HO-1, and BCL-2. In a xenograft mouse model, entinostat and fludarabine combination induced apoptosis, suggesting targeting HDAC1 as a potential approach to overcome chemotherapy resistance in TP53-mutated CLL [32]. Likewise, combinatorial effects of entinostat and cladribine were investigated against multiple myeloma cells, and results revealed both agents synergistically induced anti-proliferative/anti-survival effects via down regulation of *CCND1* and *E2F* and up regulation of *P21* [31]. Similar to the present research, in the study carried out by Singh and colleagues, the bicyclic aromatic ring of entinostat was used to design and synthesize class I HDACis. In vitro enzymatic and cellular assays led to the identification of a new compound that exerted better anti-proliferative effects against human cutaneous T-cell lymphoma, leukemia, breast, cervical, colorectal, and gastric carcinomas [43]. Accordingly, quinoline-based benzamide derivatives of entinostat could be considered as potent candidates to design novel drugs for hematological neoplasms.

The present study has some limitations that warrant further investigation. While extended time-course studies would provide deeper insights into the anti-proliferative potential of entinostat and its benzamide derivatives, their intrinsic physicochemical properties pose significant challenges for prolonged in vitro exposure. Due to their relatively non-polar

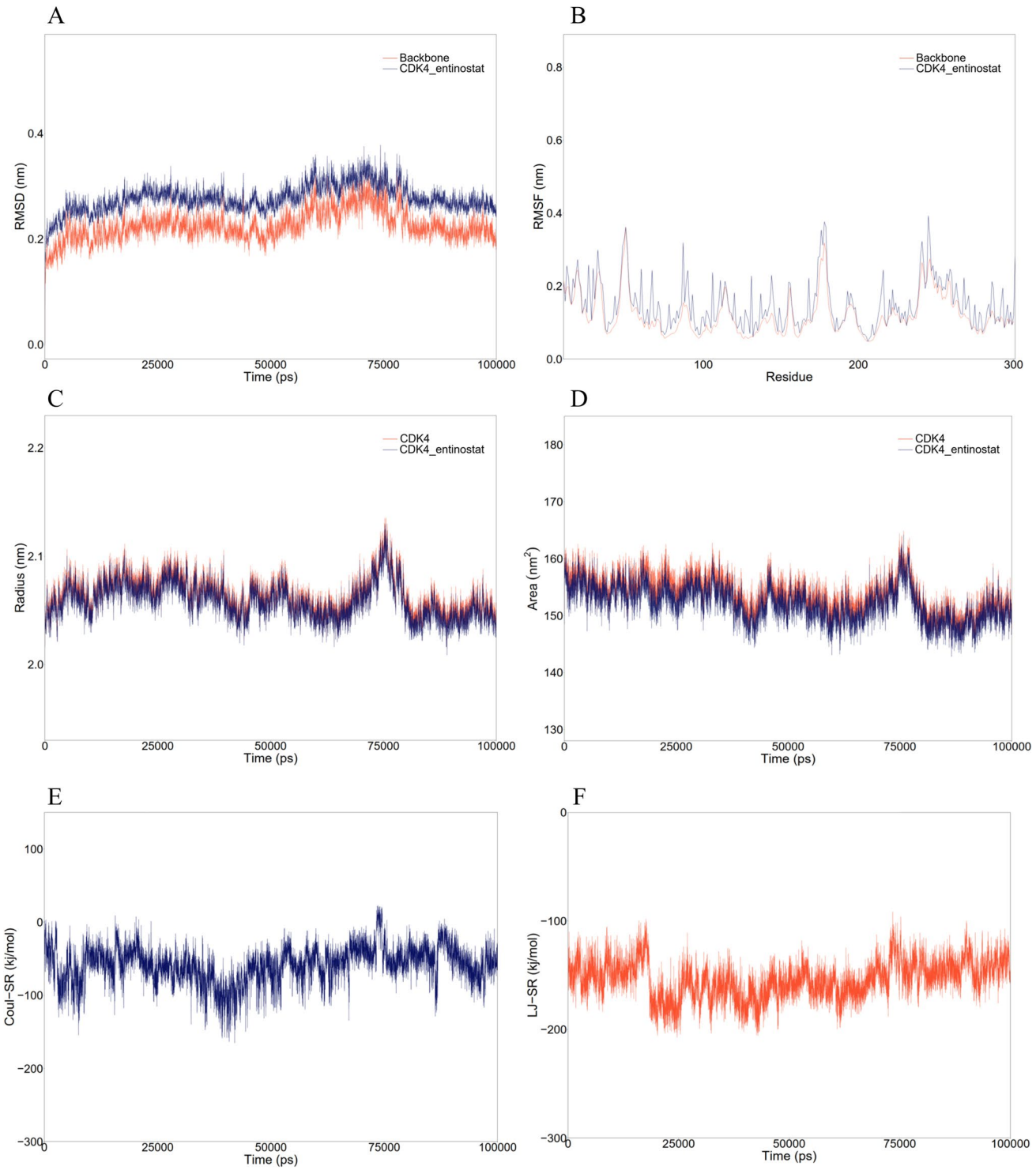

Fig. 5 Stable interaction of entinostat with CDK4. Plots generated from 100 ns molecular dynamics simulations, illustrating various structural and energetic properties of the entinostat-CDK4 complex: RMSD (**A**), RMSF (**B**), Rg (**C**), and SASA (**D**), short-range Coulombic potential (**E**) and short-range Lennard–Jones potential (**F**)

nature, these compounds exhibit limited aqueous solubility and reduced stability at time points exceeding 48 h, as observed in our preliminary 72-h treatments. This limitation constrained the feasible treatment duration (up to 48 h) and concentration range (up to 50 µM) for reliable assays in the current study. To address these challenges, future research

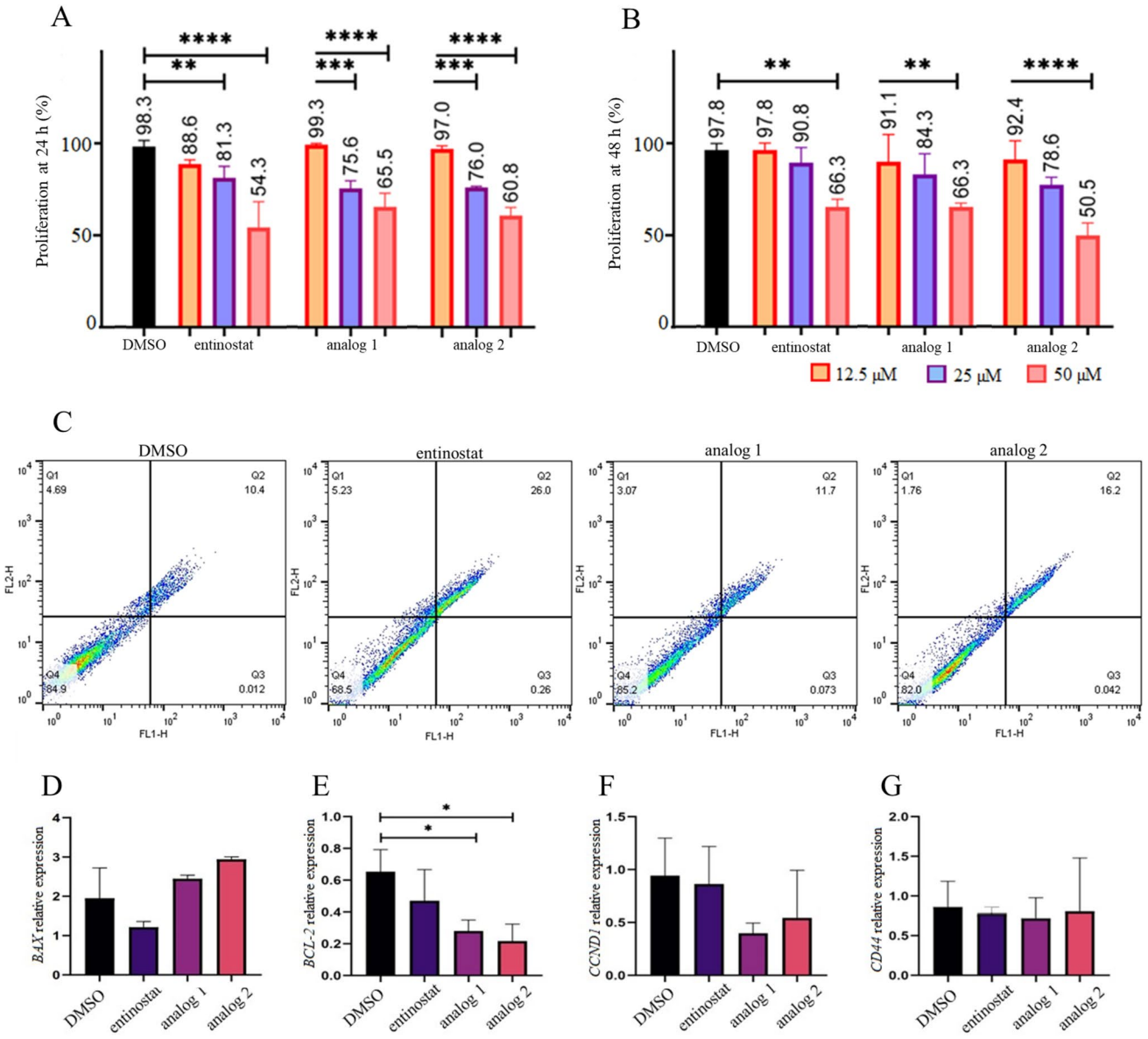

Fig. 6 Effects of entinostat and novel analogs on the proliferation, apoptosis and gene expression in MT-2 cells. Proliferation assay of MT-2 cells following treatment with entinostat, analog 1 and analog 2 for 24 h (**A**) and 48 h (**B**). Flow cytometry detection of apoptosis upon 24 h treatment of MT-2 cells with 50 µM entinostat and analogs (**C**). Cells are categorized as alive (negative for both annexin V-FITC and PI), necrotic (positive for PI only), and early or late apoptotic (positive for annexin V-FITC). Quantitative analysis of the expression of *BAX* (**D**), *BCL-2* (**E**), *CCND1* (**F**) and *CD44* (**G**). Data represent the mean ± SD from experiments performed in triplicate. Statistical significance compared to the DMSO control was determined using One-Way ANOVA, with $*p < 0.05$, $**p < 0.01$, $***p < 0.001$, and $****p < 0.0001$ indicating significance

should focus on optimizing formulation strategies-such as the use of solubilizing agents or nanoparticle-based delivery systems-to improve the solubility, stability, and bioavailability of these compounds, enabling more comprehensive evaluation over extended treatment periods. Additionally, while our study assessed proliferation markers at the mRNA level, we acknowledge the importance of validating these findings at the protein level to fully support our conclusions and recommend this as a key direction for future research.

Conclusion

Present study indicated for the first time that entinostat and novel analogs induced anti-proliferative effects on ATLL cells via interaction with CDK4 and cyclin D1, which exhibit elevated expression in ATLL cells. These findings pave the way for the development of new drugs against ATLL and provide evidence that justifies further preclinical and clinical evaluations of entinostat and its novel analogs.

Supplementary Information The online version contains supplementary material available at https://doi.org/10.1007/s12032-025-02793-3.

Author contributions S. Goudarzi and Z. Nasiri Sarvi performed in silico and in vitro experiments. R. Ghodsi provided research materials. Zeinab Noroozi drafted the initial manuscript. M.R. Keramati contributed project advice. H. Ayatollahi supervised the work. F.B. Rassouli designed, supervised, and revised the manuscript.

Funding This study was financially supported by grants from Ferdowsi University of Mashhad and Mashhad University of Medical Sciences (No. 981057).

Data availability No datasets were generated or analysed during the current study.

Declarations

Conflict of interests The authors declare no competing interests.

References

1. Nosaka K, Matsuoka M. Adult T-cell leukemia-lymphoma as a viral disease: Subtypes based on viral aspects. Cancer Sci. 2021;112(5):1688–94.
2. Oliveira PD, de Carvalho RF, Bittencourt AL. Adult T-cell leukemia/lymphoma in South and Central America and the Caribbean: Systematic search and review. Int J STD AIDS. 2017;28:217–28.
3. Ito S, Iwanaga M, Nosaka K, Imaizumi Y, Ishitsuka K, Amano M, Utsunomiya A, Tokura Y, Watanabe T, Uchimaru K, Tsukasaki K. Epidemiology of adult T-cell leukemia-lymphoma in Japan: An updated analysis, 2012–2013. Cancer Sci. 2021;112(10):4346–54.
4. Nakahata S, Enriquez-Vera D, Jahan MI, Sugata K, Satou Y. Understanding the immunopathology of HTLV-1-associated adult T-cell leukemia/lymphoma: A comprehensive review. Biomolecules. 2023;13(10):1543.
5. Rosadas C, Taylor GP. HTLV-1 and co-infections. Front Med. 2022;9: 812016.
6. Nosaka K, Crawford B, Yi J, Kuan W, Matsumoto T, Takahashi T. Systematic review of survival outcomes for relapsed or refractory adult T-cell leukemia-lymphoma. Eur J Haematol. 2022;108(3):212–22.
7. Hermine O, Ramos JC, Tobinai K. A review of new findings in adult T-cell leukemia-lymphoma: A focus on current and emerging treatment strategies. Adv Ther. 2018;35(2):135–52.
8. Tsukasaki K, Marçais A, Nasr R, Kato K, Fukuda T, Hermine O, Bazarbachi A. Diagnostic approaches and established treatments for adult T cell leukemia lymphoma. Front Microbiol. 2020;11:1207.
9. Harhaj EW, Giam CZ. NF-kappaB signaling mechanisms in HTLV-1-induced adult T-cell leukemia/lymphoma. FEBS J. 2018;285(18):3324–36.
10. Cherian MA, Baydoun HH, Al-Saleem J, Shkriabai N, Kvaratskhelia M, Green P, Ratner L. Akt pathway activation by human T-cell leukemia virus type 1 Tax oncoprotein. J Biol Chem. 2015;290(43):26270–81.
11. Matsuoka M, Yasunaga J. Human T-cell leukemia virus type 1: replication, proliferation and propagation by Tax and HTLV-1 bZIP factor. Curr Opin Virol. 2013;3(6):684–91.
12. Nicot C. HTLV-I Tax-mediated inactivation of cell cycle checkpoints and DNA repair pathways contribute to cellular transformation: "A random mutagenesis model." J Cancer Sci. 2015;2(2):6.
13. Torshizi R, Ghayour Karimani E, Etminani K, Akbarin MM, Jamialahmadi K, Shirdel A, Rahimi H, Allahyari A, Golabpour A, Rafatpanah H. Altered expression of cell cycle regulators in adult T-cell leukemia/ lymphoma patients. Rep Biochem Mol Biol. 2017;6(1):88–94.
14. Suzuki T, Kitao S, Matsushime H, Yoshida M. HTLV-1 Tax protein interacts with cyclin-dependent kinase inhibitor p16INK4A and counteracts its inhibitory activity towards CDK4. EMBO J. 1996;15(7):1607–14.
15. Fraedrich K, Müller B, Grassmann R. The HTLV-1 Tax protein binding domain of cyclin-dependent kinase 4 (CDK4) includes the regulatory PSTAIRE helix. Retrovirology. 2005;2:54.
16. Kim YM, Geiger TR, Egan D, Sharma N, Nyborg JK. The HTLV-1 Tax protein cooperates with phosphorylated CREB, TORC2, and p300 to activate CRE-dependent cyclin D1 transcription. Oncogene. 2010;29(14):2142–52.
17. Fochi S, Mutascio S, Bertazzoni U, Zipeto D, Romanelli MG. HTLV deregulation of the NF-kappaB pathway: An update on Tax and antisense proteins role. Front Microbiol. 2018;9:285.
18. Ishitsuka K, Kunami N, Katsuya H, Nogami R, Ishikawa C, Yotsumoto F, Tanji H, Mori N, Takeshita M, Miyamoto S, Tamura K. Targeting Bcl-2 family proteins in adult T-cell leukemia/lymphoma: in vitro and in vivo effects of the novel Bcl-2 family inhibitor ABT-737. Cancer Lett. 2012;317(2):218–25.
19. Witzens-Harig M, Giaisi M, Köhler R, Krammer PH, Li-Weber M. HTLV-1-associated adult T cell leukemia is highly susceptible to Navitoclax due to enhanced Bax expression. Int J Cancer. 2016;138(2):507–14.
20. Luke JJ, Van De Wetering CI, Knudson CM. Lymphoma development in Bax transgenic mice is inhibited by Bcl-2 and associated with chromosomal instability. Cell Death Differ. 2003;10(6):740–8.
21. Yang F, Zhao N, Ge D, Chen Y. Next-generation of selective histone deacetylase inhibitors. RSC Adv. 2019;9:19571.
22. Park SY, Kim JS. A short guide to histone deacetylases including recent progress on class II enzymes. Exp Mol Med. 2020;52(2):204–12.
23. Jenke R, Rebing N, Hansen FK, Aigner A, Büch T. Anticancer therapy with HDAC inhibitors: Mechanism-based combination strategies and future perspectives. Cancers. 2021;13(4):634.
24. Marks P. Discovery and development of SAHA as an anticancer agent. Oncogene. 2007;26:1351e1356.
25. Qian X, Ara G, Mills E, LaRochelle WJ, Lichenstein HS, Jeffers M. Activity of the histone deacetylase inhibitor belinostat (PXD101) in preclinical models of prostate cancer. Int J Cancer. 2008;122:1400e1410.
26. Laubach JP, Moreau P, San-Miguel JF, Richardson PG. Panobinostat for the treatment of multiple myeloma. Clin Cancer Res. 2015;21:4767e4773.
27. Lu AH, Zhou NZ, Robert MF. MGCD0103, a novel isotype-selective histone deacetylase inhibitor, has broad spectrum antitumor activity in vitro and in vivo. Mol Cancer Therapeut. 2008;7:759e768.
28. Masuda N, Tamura K, Yasojima H, Shimomura A, Sawaki M, Lee MJ, Yuno A, Trepel J, Kimura R, Nishimura Y, Saji S, Iwata H. Phase 1 trial of entinostat as monotherapy and combined with exemestane in Japanese patients with hormone receptor-positive advanced breast cancer. BMC Cancer. 2021;21:1269.
29. Wang B, Lyu H, Pei S, Song D, Ni J, Liu B. Cladribine in combination with entinostat synergistically elicits anti-proliferative/anti-survival effects on multiple myeloma cells. Cell Cycle. 2018;17(8):985–96.
30. Huang XP, Li X, Situ MY, Huang LY, Wang JY, He TC, Yan QH, Xie XY, Zhang YJ, Gao YH, Li YH, Rong TH, Wang MR, Cai QQ, Fu JH. Entinostat reverses cisplatin resistance in esophageal

squamous cell carcinoma via down-regulation of multidrug resistance gene 1. Cancer Lett. 2018;414:294–300.
31. Shin J, Carr A, Corner GA, Togel L, Dávalos-Salas M, Tran H, Chueh AC, Al-Obaidi S, Chionh F, Ahmed N, Buchanan DD, Young JP, Malo MS, Hodin RA, Arango D, Sieber OM, Augenlicht LH, Dhillon AS, Weber TK, Mariadason JM. The intestinal epithelial cell differentiation marker intestinal alkaline phosphatase (ALPi) is selectively induced by histone deacetylase inhibitors (HDACi) in colon cancer cells in a Kruppel-like factor 5 (KLF5)-dependent manner. J Biol Chem. 2014;289(36):25306–16.
32. Zhou Z, Fang Q, Li P. Entinostat combined with Fludarabine synergistically enhances the induction of apoptosis in TP53 mutated CLL cells via the HDAC1/HO-1 pathway. Life Sci. 2019;232:116583.
33. Schöning-Stierand K, Diedrich K, Ehrt C, Flachsenberg F, Graef J, Sieg J, Penner P, Poppinga M, Ungethüm A, Rarey M. ProteinsPlus: a comprehensive collection of web-based molecular modeling tools. Nucleic Acids Res. 2022;50:W611–5.
34. Flachsenberg F, Meyder A, Sommer K, Penner P, Rarey M. A consistent scheme for gradient-based optimization of protein–ligand poses. J Chem Inf Mod. 2020;60:6502–22.
35. Diedrich K, Krause B, Berg O, Rarey M. PoseEdit: enhanced ligand binding mode communication by interactive 2D diagrams. J Comput Aided Mol Des. 2023;37:491–503.
36. Stierand K, Maass PC, Rarey M. Drawing the PDB - protein-ligand complexes in two dimensions. Med Chem Let. 2010;1(9):540–5.
37. Omidkhah N, Eisvand F, Hadizadeh F, Zarghi A, Ghodsi R. Synthesis, cytotoxicity, pan-HDAC inhibitory activity and docking study of N-(2-Aminophenyl)-2-arylquinoline-4- and N-(2-Aminophenyl)-2-arylbenzo[h]quinoline-4-carboxamides. Chem Select. 2022;7(29):e202201239.
38. Omidkhah N, Hadizadeh F, Abnous K, Ghodsi R. Synthesis, structure activity relationship and biological evaluation of a novel series of quinoline–based benzamide derivatives as anticancer agents and histone deacetylase (HDAC) inhibitors. J Mol Struct. 2022;1267:133599.
39. Chueh AC, Tse JW, Togel L, Mariadason JM. Mechanisms of histone deacetylase inhibitor-regulated gene expression in cancer cells. Antioxid Redox Signal. 2015;23(1):66–84.
40. Copeland A, Buglio D, Younes A. Histone deacetylase inhibitors in lymphoma. Curr Opin Oncol. 2010;22:431–6.
41. Jona A, Khaskhely N, Buglio D, Shafer JA, Derenzini E, Bollard CM, Medeiros LJ, Illés A, Ji Y, Younes A. The histone deacetylase inhibitor entinostat (SNDX-275) induces apoptosis in Hodgkin lymphoma cells and synergizes with Bcl-2 family inhibitors. Exp Hematol. 2011;39(10):1007-1017.e1.
42. Zhou L, Ruvolo V, Mcqueen T, Chen W, Samudio IJ, Conneely O, Konopleva M, Andreeff M. HDAC inhibition by SNDX-275 (Entinostat) restores expression of silenced leukemia-associated transcription factors Nur77 and Nor1 and of key pro-apoptotic proteins in AML. Leukemia. 2013;27(6):1358–68.
43. Singh A, Chang TY, Kaur N, Hsu KC, Yen Y, Lin TE, Lai MJ, Lee SB, Liou JP. CAP rigidification of MS-275 and chidamide leads to enhanced antiproliferative effects mediated through HDAC1, 2 and tubulin polymerization inhibition. Eur J Med Chem. 2021;215:113169.